

Check for updates



Intracellular Detection of *C. acnes* and *S. aureus* in Non-Herniated Human Intervertebral Discs: Implications for Catabolic Signaling Pathways

Andrea Nüesch¹ | Exarchos Kanelis^{2,3} | Leonidas G. Alexopoulos^{2,3} | Benjamin Gantenbein^{4,5} | Melissa Lacey⁶ | Christine L. Le Maitre¹ |

¹Division of Clinical Medicine, School of Medicine and Population Health, University of Sheffield, UK | ²School of Mechanical Engineering, National Technical University of Athens, Zografou, Greece | ³Protavio Ltd, Science Park Demokritos, Agia Paraskevi, Greece | ⁴Tissue Engineering for Orthopaedics & Mechanobiology, Bone & Joint Program, Department for BioMedical Research (DBMR) of the Faculty of Medicine of the University of Bern, University of Bern, Bern, Switzerland | ⁵Department of Orthopaedic Surgery and Traumatology, Inselspital, Bern University Hospital, Medical Faculty, University of Bern, Bern, Switzerland | ⁶School of Biosciences and Chemistry, Sheffield Hallam University, Sheffield, UK

Correspondence: Christine L. Le Maitre (c.lemaitre@sheffield.ac.uk)

Received: 4 July 2025 | Revised: 21 October 2025 | Accepted: 29 October 2025

Funding: Financial support was received from the Marie Skłodowska Curie International Training Network (ITN) "disc4all" (https://disc4all.upf.edu, accessed on 10 May 2022) grant agreement #955735 (https://cordis.europa.eu/project/id/955735, accessed on 26 Sept 2024).

ABSTRACT

Objective: To investigate whether the presence of bacteria within non-herniated intervertebral discs (IVDs) represents bacterial antigen signals within disc cell boundaries, consistent with in vivo presence and to assess the effects of bacterial exposure on human nucleus pulposus (NP) cells, focusing on immune response pathways and catabolic factor expression.

Methods: Non-herniated IVD tissue was analyzed using immunohistochemistry (n = 79 discs) to detect bacterial presence and its correlation with catabolic factors. Bacterial survival was tested under IVD-like conditions to simulate intradiscal growth potential. Human NP cells were treated with bacterial cell membrane components in both monolayer (n = 3) and 3D cultures (n = 3), with secretome analyzed via Luminex profiling. Co-culture studies investigated bacterial internalization, with NP cells exposed to peptidoglycans or co-cultured with *S. aureus* or *C. acnes* at physiologically relevant multiplicities of infection (MOI 0.01, n = 3) to assess intracellular signaling activation.

Results: Immunohistochemical analysis revealed significant correlations between *C. acnes* intracellular staining and expression of catabolic markers: MMP-3 ($p=3.39\times10^{-4}$); GSDMD (p=0.019); and the intracellular receptor: NOD2 ($p=9.6\times10^{-5}$), implicating these factors in immune surveillance by NP cells. The presence of NOD2 suggests activation of intracellular pathways that contribute to bacterial detection and trigger inflammatory responses. Stimulation of NP cells with peptidoglycan induced a strong catabolic secretome in both 2D and 3D cultures, whilst LPS showed limited effects. Low infectivity of NP cells with *C. acnes* and *S. aureus* suppressed VEGF, CXCL10 and CCL5. Effects of peptidoglycan and bacterial co-culture were altered by TLR2/NOD2 inhibition, suggesting receptor-specific but incomplete pathway dependence.

Conclusion: This study identifies key bacterial receptors and signaling pathways in the IVD in response to bacteria, highlighting potential targets for therapeutic intervention in disc-related inflammatory conditions. Our findings support the concept of an active immune role of NP cells in response to bacterial presence, challenging the notion of the disc as a sterile environment.

This is an open access article under the terms of the Creative Commons Attribution-NonCommercial License, which permits use, distribution and reproduction in any medium, provided the original work is properly cited and is not used for commercial purposes.

© 2025 The Author(s). JOR Spine published by Wiley Periodicals LLC on behalf of Orthopaedic Research Society.

1 | Introduction

The intervertebral disc (IVD) is crucial for spine flexibility and load distribution across vertebral segments [1]. Degeneration of the IVD is strongly linked to low back pain (LBP), a major cause of disability worldwide, affecting around 619 million people, particularly women [2]. Traditionally, the IVD's avascular nature suggested it was sterile, but this was challenged when Stirling et al. detected anaerobic bacteria, notably *Cutibacterium acnes* (*C. acnes*), in herniated discs from sciatica patients [3]. Since then, the role of bacterial presence and a possible disc-specific microbiome in disc health and pathology has spurred debate, especially regarding the association between bacterial colonization and Modic changes (vertebral endplate bone marrow lesions visible on MRI), hypothesized to be linked to bacteria in some cases [4, 5].

Advances in detection methods, particularly next-generation sequencing (NGS), have enabled microbiome studies in low-biomass environments like the IVD. Some findings support a unique disc microbiome [6, 7], but concerns about the contamination of biopsies collected perioperatively hinder conclusive findings. Among the detected bacteria, *C. acnes* has garnered significant attention due to its role as a skin commensal and potential opportunistic pathogen in infections, including those related to medical devices [8, 9]. Additionally, *Staphylococcus aureus* (*S. aureus*) and coagulase-negative staphylococci have been identified in disc samples [4].

Research has focused on bacterial presence in the IVD and potential signaling pathways activated by bacterial stimulation. Pattern recognition receptors (PRRs) such as toll-like receptors (TLRs) and nucleotide oligomerisation domain-like receptors (NLRs) detect molecular patterns associated with pathogens and cellular damage, mediating immune responses. TLR2 and TLR4, which recognize bacterial components, have been detected in human IVD cells [10, 11]. TLR2, upregulates catabolic factors in response to Gram-positive bacteria, including C. acnes [12]. Whilst TLR4 is activated by Gram-negative bacteria [13]. NLRP3 a member of the NLR family is expressed by NP cells and mediates C. acnes-induced pyroptosis [14], however NOD2, which also detects Gram-positive bacteria, has not been investigated in the IVD [15]. In this context, we selected peptidoglycan (PGN) and lipopolysaccharide (LPS) as prototypical bacterial ligands to probe NP cell responsiveness. PGN is a Gram-positive wall component that engages the TLR2/NOD2 axis, whereas LPS from Gram-negative bacteria activates TLR4. Testing these ligands therefore provides mechanistic insight into the role of distinct PRR pathways in disc cell signaling.

This study aimed to investigate potential bacterial presence within non-herniated human IVDs, distinguishing perioperative contamination from in vivo colonization, and to examine correlations between PRRs, catabolic factors, and bacterial presence. Additionally, bacterial growth in IVD-mimicking conditions was determined, together with the impact of bacterial exposure on disc cells, focusing on signaling pathways.

2 | Methods

2.1 | Experimental Design

This study initially investigated whether bacteria could be detected within non-herniated human IVDs using immunohistochemistry to enable localization of bacteria and determine whether bacterial presence was likely due to contamination alone or could represent in vivo disc bacteria (Figure S1). Bacterial growth was also assessed under conditions mimicking the harsh disc environment to monitor their survival. The ability of bacteria to survive and multiply within conditions that mimicked the harsh disc environment was undertaken to determine potential growth rates in vivo. Following confirmation of IHC localization for bacterial antigens within cellular boundaries within the disc, correlation with catabolic factors and the ability of bacteria to multiply within conditions that mimicked the disc environment, the potential direct effects of bacteria were investigated in vitro. Initial studies utilized human nucleus pulposus (NP) cells in monolayer and subsequently in a 3D culture system treated with bacterial cell membrane components to determine their influence on cellular secretome, which was analyzed using a Luminex assay. Co-culture studies were then utilized to determine the time course of bacterial internalization into human NP cells. Finally, NP cells were treated with peptidoglycans (PGNs) or in co-culture with physiologically relevant multiplicity of infection (MOI) of S. aureus or C. acnes to determine activation of intracellular signaling pathways and modulation of secretome. These cultures were performed with and without the presence of inhibitors of TLR2 and NOD receptors to determine potential receptor-mediated responses.

2.2 | Tissue Collection

Human IVD tissue was collected from patients who gave their consent during spinal surgery at Northern General Hospital or Claremont Hospital in Sheffield (UK) (Tables S1 and S3). Local ethics approval was given for this work by Sheffield Research Ethics Committee (09/H1308/70) (IRAS approval: 10226). The tissue was placed into 30 mL low glucose (1.0 g/L) Dulbecco's Modified Eagle Medium DMEM (LG-DMEM, Invitrogen 31600-083, Paisley, UK) supplemented with 1% Penicillin/ Streptomycin (P/S, Invitrogen, 15070-063) and 25 µg/mL Amphotericin B (Sigma, A2942, Dorste, Gillingham, UK) at 4 degrees at surgery, and transported under sterile conditions to the laboratory. As a first step the tissue was washed twice in sterile phosphate buffered saline (PBS, OXOID BR0014G, Thermo Fisher Scientific, Loughborough, UK) before splitting the tissue into annulus fibrosus (AF), cartilaginous endplate (CEP), and NP tissues. For cell isolation solely NP tissue was used in this study whereas parts from all tissue components (where available), were fixed in 10% (w/v) formalin (Leica, Milton Keynes, UK), processed, embedded in paraffin wax to perform histological grading of degeneration and immunohistochemical staining.

2.3 | Hematoxylin and Eosin Staining and Grading for State of Degeneration

Sections were cut with a microtome at a thickness of $4\mu m$, and mounted on positively charged slides (Superfrost Plus,

Epredia, Runcorn UK). Sections were dewaxed in sub-X (Leica Microsystems) 3×5min and hydrated in industrial methylated spirit (IMS, 3×5min). Sections were then stained with Harris's hematoxylin (Surgipath Europe Ltd) for 5min and blued for 3min under running tap water. For counterstaining alcoholic eosin (Leica Microsystems) was applied for 2min. After dehydration in IMS and clearing in sub-X the slides were mounted using Pertex (Leica Microsystems). Grading was performed following the standardized histopathology scoring system for human IVD degeneration [16]. For samples consisting of both NP and AF, the average of the two scores was taken as the degenerative score. CEPs were excluded from the analysis as they were observed in low numbers of samples.

2.4 | Immunohistochemical Staining (IHC)

Human IVD specimens (Table S1) were fixed in 10% (w/v) formalin for 48h up to a week and embedded in paraffin wax. Sections were cut with a microtome at a thickness of 4 µm whereby sections were first cut into the block to avoid edges of tissues and mounted on positively charged slides. Immunohistochemical staining was performed as previously published [17]. The sections were de-waxed, rehydrated and endogenous peroxidases were blocked for 60 min in 100% IMS containing 3% (v/v) hydrogen peroxide (Sigma Aldrich) and 0.06% (v/v) concentrated HCl. Antigen retrieval depended on the antibody (Table S2) and consisted either of no antigen retrieval, enzyme antigen retrieval $[0.1\% \text{ w/v} \alpha$ chymotrypsin (Sigma Aldrich, Poole, UK) in tris-buffer saline (TBS) (20 mmol/L Tris, 150 mmol/L NaCl pH 7.5) containing 0.1% w/v CaCl, for 30 min at 37°C or heat antigen retrieval [0.05 M Tris, pH 9.5 preheated on automatic cook mode prior to 5 min incubation of samples within a rice steamer on warm (ASAB, AS-40979, UK)]. Following antigen retrieval, the sections were washed in TBS and non-specific antibody binding was blocked (Table S2) for 1 h at room temperature in 1% (w/v) bovine serum albumin (BSA) containing 25% (v/v) normal serum in TBS. Primary antibodies (Table S2) were applied to the slides overnight at 4°C diluted in TBS containing 1% (w/v) BSA. Simultaneously IgG controls in place of the primary antibodies were used at equal protein concentrations to test for non-specific binding of the isotype. Following the overnight incubation, the sections were washed with TBS three times prior to the application of the secondary antibodies at room temperature for 30 min followed by three more TBS washes, before applying EliteABC reagent (Vector, Laboratories, Peterborough, UK) to the slides for 30 min. After another 3 TBS washes 0.65 mg/mL 3,3'-diaminobenzides tetrahydrochloride (DAB, Sigma-Aldrich) containing 0.08% (v/v) H₂O₂ in TBS was added for 20 min, prior to washes in running tap water for 5 min. Counterstaining of the nuclei was performed with Hematoxylin (Gill's Hematoxylin GHS232, Sigma, Dorset, UK) for 20s and blued for 3 min under running tap water. After dehydration in graded ethanol and clearing in xylene the slides were mounted using Pertex. Slides were scanned at 20x and 40× magnification using a slidescanner (PANNORAMIC 250 Flash II DX, 3DHistech) and representative images included to highlight immunohistochemical staining. Image analysis of the combined NP and AF tissues was performed using the semi-automatic quantification protocol, whereby tissue edges were excluded from analysis [18].

2.5 | Isolation and Expansion of Human Nucleus Pulposus (NP) Cells

Cell isolation (Table S3) was performed using the standardized protocol as previously published [19]. Briefly, upon washing with PBS, the tissue was transferred into a 50 mL falcon tube containing 20 mL of Collagenase type II (285.00 units/mg, 0.05 mg/mL, Invitrogen: 17101-015) and incubated (37°C, 5% CO₂, 21% O₂) for 4h on an orbital shaker. The released cells were filtered through a 70 µm cell strainer, counted, and plated at a seeding concentration of 10000 cells/cm². Culture media composed of high glucose (4.5 g/L) DMEM Medium (HG-DMEM, Invitrogen: 10569010 HG) supplemented with 10% (v/v) heatinactivated foetal calf serum (FCS, LifeTechnologies, Paisley, UK), 1% P/S, 1% L-Glutamine (Invitrogen: 25030-024), $2.5\,\mu\text{g}/$ mL Amphotericin B and 25 μg/mLL-ascorbic acid 2-Phosphate (AA, Sigma, A5960) was added and changed 3 times per week. At 80% confluence cells were detached using Trypsin-EDTA (Invitrogen, 25300-062) and passaged 1:3. Upon passage 2, cells were used for experiments in monolayer or resuspended in 1.2% alginate to enable re-differentiation to NP phenotype.

2.6 | Encapsulation of NP Cells in Alginate

Following trypsinisation, cell suspensions were centrifuged at 400g for 4min. The cell pellet was then resuspended in culture media and counted using a NucleoCounter NC-2000. Following further centrifugation at 400g, cells were resuspended at 1.2% medium viscosity sodium alginate (Sigma A2033) in 0.15M sodium chloride (NaCl) at 4×106 cells/ml density. The resulting cell suspension was passed through a 21gauge needle into 24 well plates containing 200 mM calcium chloride (CaCl₂), six beads per well. Beads were incubated for 10 min at 37°C in 200 mM CaCl₂, followed by 2 washes of 0.15 M NaCl and media. Two milliliters of complete low glucose (LG, 1g/L) culture media: LG DMEM, supplemented with 1% insulin transferrin selenium-x (ITS-x, Invitrogen, 51 500-056), 1% P/S, 1% L-Glutamine, 2.5 μg/mL Amphotericin B, 25 μg/mL AA, 40 µg/mLL-Proline and 1.25 mg/mL Albumax were added [20]. Cultures were maintained for 2 weeks at 37°C under physioxia conditions (5% O_2 , 5% CO_2) to regain in vivo phenotype.

2.7 | Bacterial Cultures

Staphylococcus aureus SH1000 a derivative of the 8325–4 strain and Cutibacterium acnes (NCTC 737, Culture Collection UK Health Security Agency, Salisbury, UK) were used for this study. S. aureus was grown on Mueller Hinton agar (70191, Merck, Dorset, UK) plates at 37 degrees and 21% $\rm O_2$ overnight. C. acnes was grown at 37 degrees in an anaerobic chamber on agar plates for 1 week. Liquid cultures were grown under 5% $\rm O_2$ by adding one colony-forming unit (CFU) to 4mL of complete LG media. S. aureus was used after 16 h of culture, while C. acnes was cultured for 48 h prior to use.

JOR Spine, 2025 3 of 15

2.8 | Bacterial Growth

Bacterial growth was measured at 5% O2 within 3 different culture media. Mueller Hinton Broth was used as a positive control, whilst complete LG-culture media at an osmolarity of 350 mOsm/Kg and 450 mOsm/Kg were used to represent the disc environment, as these values reflect the physiological osmotic pressures reported for healthy and degenerated IVD tissue [21]. OSM was adjusted using the impermeant cation N-methyl-D-glucosamine HCl to prevent solute-specific target effects from other compounds and resulting OSM confirmed by freezing point depression using Model 3320 osmometer (Advanced Instruments, Dorset, UK). An initial liquid culture in the respective culture media was diluted to have an optical density of 0.1 at a wavelength of 600 nm. The suspended bacteria were then seeded into a 96-well plate, and the optical density was measured with the Stratus kinetic microplate reader (Cerillo, Charlottesville, VA 22902, USA). A second 96-well plate was used to prepare serial dilution to count CFU every hour for S. aureus and twice a day for C. acnes.

2.9 | Co-Culture of Human NP Cells and S. aureus

Human NP cells were seeded into chamber slides at 0.3×10^5 cells/well in LG-culture media. Cells were left to attach overnight at 37°C, 5% CO₂, 21% O₂, whilst *S. aureus* was grown in a liquid culture in LG-culture media overnight. Two hours before usage, NADA green (0.5 mM, Cat 6648, TOCRIS) was supplemented with the media labelling the peptidoglycans in the live bacteria. Fresh media, supplemented with *S. aureus* at an MOI of 0.01, was added to the cell culture and incubated for 1 h prior to fixation in 10% (w/v) formalin for 20 min. Cells were then stained with Phalloidin (A12381, Thermo Fisher) for 30 min prior to washing with PBS and mounting with gold antifade mountant with DNA stain DAPI (P36931, Thermo Fisher). Imaging was performed on a Zeiss LSM 800 confocal microscope (Carl Zeiss Microscopy GmbH, Oberkochen, Germany).

2.10 | Stimulation With Peptidoglycans (PGN) and Lipopolysaccharides (LPS)

Following trypsinisation and counting, cells were seeded into a 12-well plate at a concentration of 0.5×10^6 cells/well for the monolayer culture. Cultures were held at 37° C, 5% CO $_2$, 21% O $_2$. After an initial settling period of 24h in complete LG media, the cells were treated for 48h with different concentrations $(0-50\,\mu\text{g/mL})$ of PGN and lipopolysaccharides (LPS) respectively. Media was collected following treatment for protein analysis with Luminex immunoassay. Cells in alginate were cultured under physioxia conditions (5% O $_2$, 5% CO $_2$) in complete LG media supplemented with different concentrations of PGN $(0-50\,\mu\text{g/mL})$ for 72h respectively. Cells were permeabilised with 0.1% Triton X-100 in PBS for 3 min and stained with Phalloidin for 30 min.

2.11 | Inhibition of NOD and TLR2 and Stimulation With PGN, S. aureus and C. acnes

Cells from 3 human donors (Table S3) at passage 2 were trypsinised counted, and seeded into 96 well plates at a density of 15000 cells per well, and 48 well plates at a seeding density of 30000 cells per well. Cells were left to attach overnight in complete LG media under physioxia conditions (5% O₂, 5% CO₂). Cells were treated with the inhibitors for nucleotide oligomerisation domain in 1 (NODin1, 10 µM, Selleckechem, S0004), toll like receptor 2 (TLR2, 50 µM, Selleckchem, S6597) and a combination of the two for 24h prior to treatment. Optimization of the concentrations was performed by measuring the metabolic activity using a resazurin reduction assay to confirm no detrimental effects on viability. Cells were incubated for 2h at 37°C and resazurin sodium salt (119,4 µM, Sigma Aldrich, R7017) in media before absorbance was measured at excitation 560 nm and emission 590 nm. The treatment groups were stimulated with PGN (50µg/mL) for 48h or bacterial stimulation with C. acnes or S. aureus SH1000 with and without the presence of inhibitors. Bacteria were added for 2h with and without the presence of inhibitors at a ratio of 1 bacterium to 100 cells (MOI 0.01) before washing non-internalized bacteria with PBS and adding fresh media supplemented with the inhibitors to culture the cells for a further 48 h. Media were collected to perform Luminex analysis.

2.12 | Cell Based Phosphorylation Measurements

Protein phosphorylation was measured for c-Jun-N-terminal kinase (JNK, CBEL-JNK-1, RayBiotech, GA 30092, US) p38 mitogen-activated protein kinase (p38, CBEL-P38, RayBiotech), extracellular signal-regulated kinase (ERK, CBEL-ERK, RayBiotech) and nuclear factor kappa Bp65 (NFkB, FBCAB0073, Assay Genie, Dublin Ireland) as per the manufacturer's instructions. As previously stated, cells were seeded into the 96 well plates and incubated overnight before applying inhibition followed by the treatment. After 2h of treatment, following the manufacturer's instructions, the cell culture medium was discarded and washed 3 times with the provided wash buffer before fixing the cells for 20 min. Following the manufacturer's instructions for kits purchased from RayBiotech (CBEL-JNK-1, CBEL-P38, CBEL-ERK) the absorbance for the phosphorylated and nonphosphorylated forms of the target protein was measured in two identically treated wells. For the NFkB p65 kit, in addition to measuring the phosphorylated and non-phosphorylated targets, GAPDH was measured in each well.

2.13 | Luminex

Conditioned media from the initial LPS and PGN treatment was collected and analyzed for 73 secreted proteins for monolayer culture (Table S4, 2D) and 28 proteins for alginate bead culture (Table S4, 3D) using bead-based Luminex multiplex immunoassays (Protavio, Athens, Greece), as described previously [22]. Six assay panels were employed to measure the 73 analytes in the conditioned media, utilizing an eight-point standard curve. Ninety-six well plates were coated with $50\,\mu\text{L}$

of each 1x bead mix dilution (Mag-Plex magnetic microspheres, Luminex Corp, Austin, TX, USA), containing 2500 beads per bead ID, and incubated with 35 µL of standards, samples, and blanks for 90 min at room temperature on an orbital shaker (1000 rpm). Wells were washed twice with assay buffer (PR-ASSB-1x, Protavio, Greece), followed by the addition of 20 µL of a detection antibody mix at an average concentration of 1 µg/mL to each well, and incubated for 60 min at room temperature on an orbital shaker (1000 rpm). After two more washes with assay buffer, 35 µL of Streptavidin-R-Phycoerythrin conjugate (5 µg/mL, SAPE-001, MOSS, USA) was added and incubated for 15 min under the same conditions. Finally, the wells were washed twice and resuspended in 130 µL of assay buffer, and the median fluorescence intensity (MFI) values were measured using the Luminex FLEXMAP 3D platform (Luminex Corp., Austin, TX, USA) with a minimum of 100 bead counts per sample.

For the Luminex analysis performed on the study of treatment with PGN, *S. aureus* or *C. acnes* with or without inhibitors a reduced panel was used based on results from the first study (Table S4). The analysis was performed in Sheffield, using R&D Systems' Luminex assay (LXSAHM-20, R&D Systems, Minneapolis, US) following the manufacturer's instructions. The median MFI values were measured utilizing Luminex 200, Thermo Scientific with a minimum of 50 bead counts per sample.

The two Luminex assays (Protavio/FLEXMAP 3D and R&D Systems/Luminex 200) were conducted independently and not cross-linked. All analyses were performed separately within each platform, without pooling or direct quantitative comparison between assays.

2.14 | Statistical Analysis

Statistical analysis for IHC positivity rates was conducted using GraphPad Prism (Version 10.3.1509). A Kruskal-Wallis test with Dunn's multiple comparisons was used to compare different groups for each antibody staining. Normality of correlation data was assessed using the Shapiro-Wilk test. As data were normally distributed, a two-tailed Pearson correlation analysis with a 95% confidence interval was performed to assess the correlation between positivity rates for various antibodies. For the comparison between bacterial cell wall component treatments and the control group, data were firstly normalized to donor controls and statistical analysis conducted in GraphPad Prism v.10.6.1. Data were shown to be nonparametric and as such to generate Volcano plots comparing LPS and PGN stimulation to untreated controls using Multiple Mann-Whitney testing, p values were corrected for multiple comparisons using the Holm-Sidak Method. Additionally, differences in cytokine expression levels between PGN- and bacteria-stimulated samples, with or without inhibition, were analyzed using Kruskal-Wallis Dunn's multiple comparisons in GraphPad Prism. A p value of \leq 0.05 was considered statistically significant. Experiments were conducted in biological triplicates unless stated differently. For in vitro experiments, cells from three independent donors were used, with three wells per donor analyzed independently (technical duplicates

per well were combined), giving a total of nine experimental replicates (n = 9; 3 donors \times 3 wells).

3 | Results

3.1 | *C. acnes* and *S. aureus* Were Present in Non-Herniated Human IVD Samples

C. acnes (detected with an antibody to C. acnes lysate) and S. aureus were investigated in human IVD samples using immunohistochemical staining (Figure 1A). C. acnes was detected in all the samples ranging from 5.9%-99.6% of cells with immunopositivity staining (n=79), average positivity rate $68.15\% \pm 26.6\%$ (Figure 1B). No statistically significant difference was observed between age groups, degeneration grade or presence of Modic change (Figure 1). S. aureus was detected in 38 out of 78 IVDs ranging from 0.6% to 7.6% (average positivity rate $1.9\% \pm 1.4\%$). Samples from female (f) patients showed a higher abundance of S. aureus than samples from male (m) patients (f = 60.5% (26/43), m = 47.8% (11/23)). No difference was observed with age, degeneration state or type of Modic change. C. acnes and S. aureus immunopositivity were solely detected within cellular boundaries and not as biofilms within the tissue (Figure 1). To conclude, both C. acnes and S. aureus immunopositivity were identified within cellular boundaries of non-herniated IVDs, with C. acnes showing higher prevalence.

3.2 | TLR2, TLR4 and NOD2 Are Expressed in Human IVD Samples; NOD2 Presence Correlates With the Positivity Rate of *C. acnes*, TLR2 and TLR4

Immunohistochemical staining confirmed the presence of TLR2 (average positivity rate: 67.4% ±24.5%), TLR4 (average positivity rate: 28.52% ± 23.6%) and NOD 2 (average positivity rate: 28.27 ± 26.25) within human IVD tissue (Figure 2A). Pearson correlation showed a positive correlation between TLR2 and NOD2 ($p=1.58\times10^{-6}$, r=0.589), TLR4 and NOD2 $(p=1.79\times10^{-7}, r=0.576)$ and TLR2 and TLR4 $(p=2.4\times10^{-8}, r=0.576)$ r=0.622) (Figure 2B). Correlation was also detected between NOD2 and C. acnes (p=0.028, r=0.262) (Figure 2B). While other comparisons failed to show significant correlations (p>0.05) (Figure 2B). TLR4 showed significantly more immunopositively stained cells (p=0.0025) in discs at level L5/S1, compared to cervical IVDs (Figure 2C), whilst TLR2 and NOD2 did not show differential percentage immunopositivity with disc level. In summary, TLR2 was highly expressed (~67%), TLR4 and NOD2 were present in ~28% of cells, and NOD2 correlated with C. acnes and both TLRs, implying coordinated receptor activity in bacterial recognition.

3.3 | Correlation Between Bacterial Components and Receptors With Catabolic Factors

Immunohistochemical staining showed the presence of catabolic factors interleukin-1 β (IL-1 β), matrix metalloproteinase 3 (MMP-3), a disintegrin and metalloproteinase with thrombospondin motifs 4 (ADAMTS4) and gasdermin-D (GSDMD)

JOR Spine, 2025 5 of 15

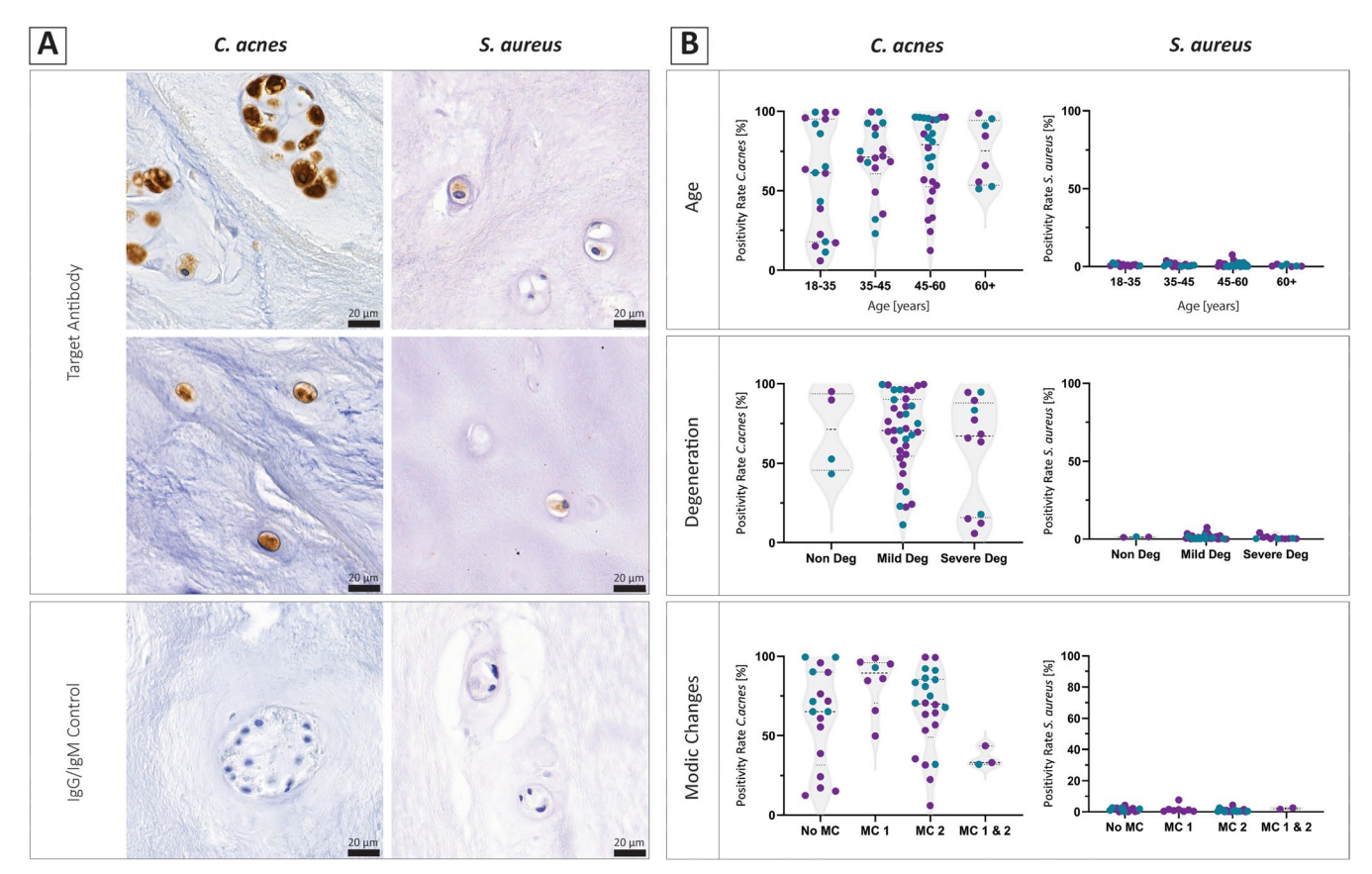


FIGURE 1 | *C. acnes* and *S. aureus* are present within non-herniated human IVDs. (A) Immunohistochemical staining for *C. acnes* lysate and *S. aureus* in human IVD tissue. Brown staining confirms the presence of the target antigen, whilst the only blue IgG/IgM control shows no unspecific binding. The bacteria were only detected within cellular boundaries and not as biofilm within the tissue (B) Positivity rate of *C. acnes* and *S. aureus* in each sample, separated according to age (years) (top), the histological state of degeneration (middle), (whereby non degenerate is classified as histological grade of degeneration between 0 and 3, mild degeneration is classified as histological grade of degeneration between 4 and 6 and severe degeneration histological score between 7 and 9), and the type of Modic changes (bottom). The different colors purple and blue represent female and male tissue donors respectively. Statistical analysis was performed using Kruskal-Wallis multiple comparison.

(Figure S2). Pearson correlation between age, degenerative state, different catabolic factors and bacteria and their receptors showed a positive correlation between the patients' age and C. acnes (p = 0.048, r = 0.235) (Figure 3). Histological grade of degeneration did not show any correlation with the catabolic factors, the presence of bacteria or the expression of TLR2, TLR4 and NOD2. IL-1 showed a moderate positive correlation with MMP3 ($p=7.03\times10^{-6}$, r=0.518) and TLR4 $(p=2.1\times10^{-6}, r=0.539)$ as well as a weak positive correlation with NOD2 ($p = 2.6 \times 10^{-5}$, r = 0.483), TLR2 ($p = 2.06 \times 10^{-4}$, r = 0.455) GSDMD (p = 0.004, r = 0.371) and ADAMTS4 (p=0.031, r=0.263) (Figure 3). MMP3 showed a moderate positive correlation with NOD2 ($p=6.56\times10^{-9}$, r=0.649), and GSDMD (p = 0.001, r = 0.426), C. acnes ($p = 3.39 \times 10^{-4}$, r=0.431), TLR2 (p=0.02, r=0.400), and TLR4 (p=0.04, r = 0.424). ADAMTS4 correlated with TLR2 (p = 0.002, r = 0.406), TLR4 (p = 0.011, r = 0.319) and NOD2 ($p = 9.6 \times 10^{-5}$, r=0.465). Pyroptosis marker GSDMD correlated with C. acnes (p = 0.019, r = 0.298) and NOD2 (p = 0.022, r = 0.288) (Figure 3). Overall, C. acnes positivity correlated moderately with MMP3 (r = 0.43) and GSDMD (r = 0.30), while NOD2 correlated strongly with MMP3 (r = 0.65).

3.4 | PGN Stimulation Induces a Catabolic Response in Human NP Cells

The levels of cytokines and chemokines in the collected media were measured using the Luminex 73-plex assay, to determine the secretome of NP cells in monolayer culture exposed to bacterial cell wall components. Demonstrating a dose-dependent increase in catabolic cytokines, degrading enzymes and their inhibitors, neurotrophic and angiogenic regulators, anti-inflammatory cytokines, immune regulators, and chemokines following treatment with PGN but limited effects were seen following LPS stimulation (Figure 4). Whereby 5 µg/mL LPS stimulation failed to induce any significant changes in the secretome of NP cells following multianalyte analysis (Figure 4A), following 50 µg/mL a significant increase in IL-6 and NGF was seen compared to unstimulated controls (Figure 4B) (Adjusted p < 0.05). Whilst treatment of NP cells in monolayer with 5 µg/mL of PGN led to a significant increase in numerous cytokines and chemokines (IL-4, IL-5, IL-6, IL-7, IL-9, IL-13, IL-17F, IL-18, IL-22, TNF, CXCL12, GM-CSF, CTACK, DEFB1, IFNγ, FGF) (Figure 4C) (Adjusted p < 0.05). At a higher dose of $50 \mu g/mL$ PGN, there

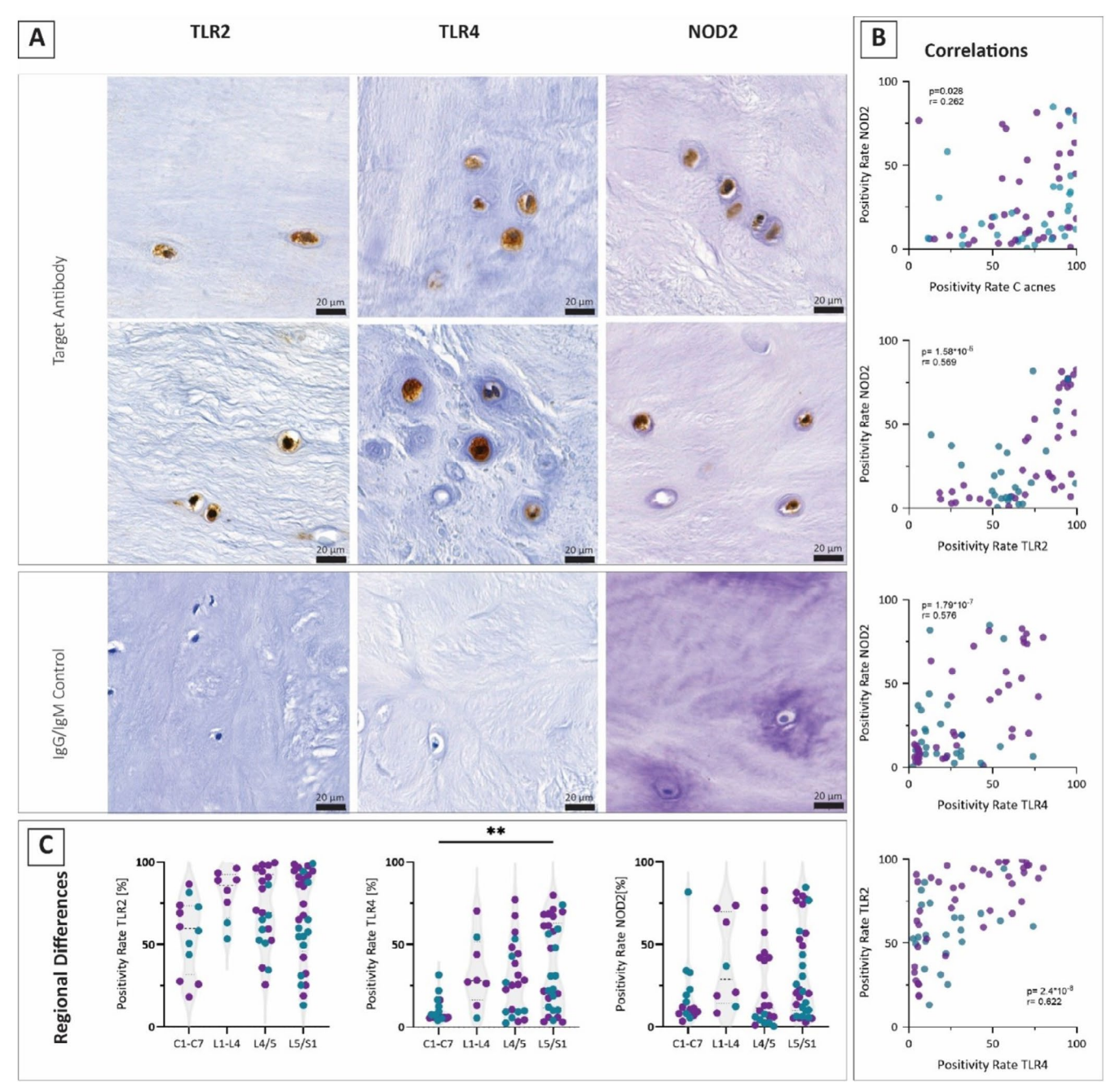


FIGURE 2 | Expression of TLR2, TLR4 and NOD2 within human IVD samples. (A) Immunohistochemical staining for TLR2, TLR4 and NOD2 confirmed their presence within the human IVD. The brown staining shows the presence of the target antigen whilst the blue IgG/IgM controls confirm only specific binding occurred. (B) Pearson correlation was performed between *C. acnes* lysate, *S. aureus*, LTR2, TLR4 and NOD2. A correlation was observed between *C. acnes* and NOD2, TLR2 and NOD2, TLR4 and NOD2 and between TLR2 and TLR4 (p = 0.05). (C) Graphs showing regional differences for TLR2, TLR4 and NOD2. Purple dots represent samples obtained from female patients, blue dots from male patients. The samples were sorted according to their disc levels from C1-C7, L1-L4, L4/5 and L5/s1. TLR4 was significantly higher on the level L5/S1 compared to the cervical discs (C1-C7). Statistical analysis was performed using Kruskal-Wallis.

was an increase in the majority of secreted factors investigated (Figure 4Di,ii). These included anti-inflammatory cytokines (IL-1Ra, IL-2Ra, IL-4, IL-10, IL-11, IL-13, IL-22, LIF), cytokines (IL-1 α , IL-1 β , IFN α 2, IFN γ , IL-5, IL-6, IL-7, IL-8, IL-9, IL-12, IL-15, IL-16, IL-17A, IL-17F, IL-18, IL-20, ST2, TNF, TNF-10, TWEAK), chemokines (CCL2, CCL3, CCL4, CCL19, CCL20, CCL20, CTACK, CXCL9, CXCL11, CXCL12, CXCL13, CXCL16, IP-10, RANTES, SCF, GROA), degrading enzymes (MMP1, MMP2, MMP7, MMP9, MMP13) and their

inhibitor TIMP1, neurotrophic factors (CNTF, NGF, NRG1, PAI-1, PROK1), and growth factors (DEFB1, FGF-basic, FST, G-CSF, GM-CSF, ICAM1, M-CSF, sRANK-L, VEGF, TGF β) (Figure 4D) (Adjusted p < 0.05). Furthermore, when NP cells were cultured in 3D alginate culture under low glucose and physioxia conditions stimulation with 5 μ g/mL PGN of NP cells resulted in the upregulation of IL-1 α , IL-1Ra, IL-4, IL-6, IL-8, IL-10, IL-17F, IL-20, NGF, IFN γ , G-CSF, SCF, PROK1 (Figure 4E) (Adjusted p < 0.05). Whilst 50 μ g/mL PGN of NP

JOR Spine, 2025 7 of 15

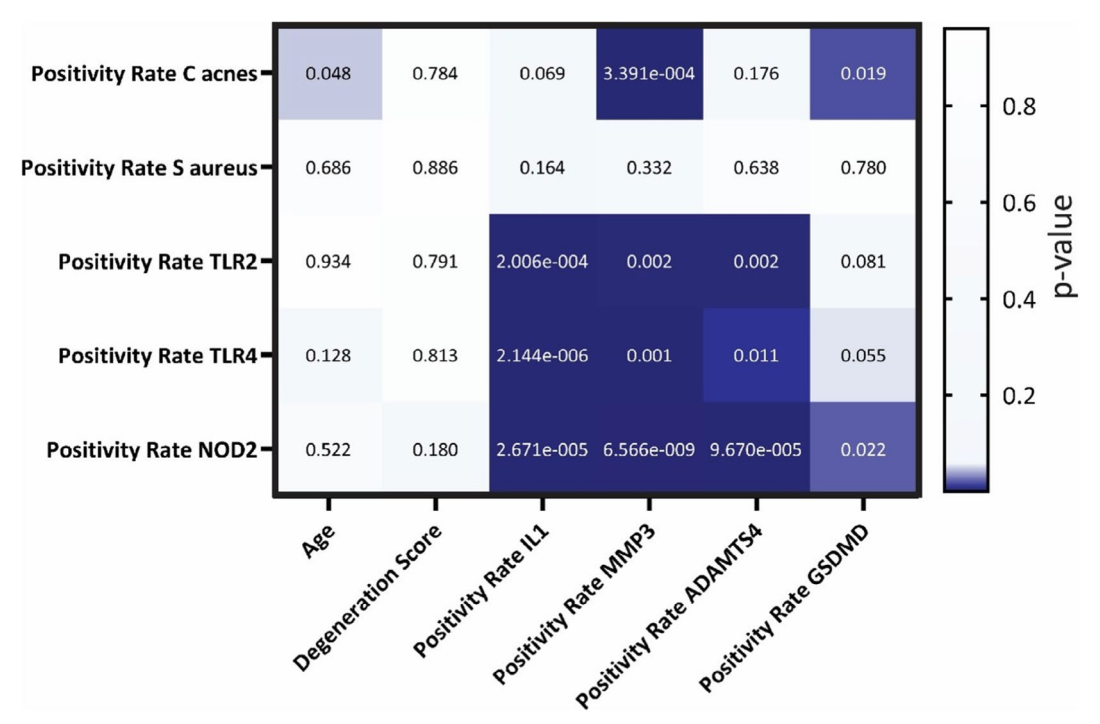


FIGURE 3 | Pearson correlation plotting the p value. Pearson correlation between the factors age, degeneration score, catabolic factors and the abundance of the bacteria C. acnes and S. aureus as well as the different receptors TLR2, TLR4 and NOD2, all spinal levels are pooled for analysis. Darker colors indicate a lower p value. (p = 0.05).

cells resuspended in alginate resulted in the upregulation of IL-1 α , IL-1Ra, IL-4, TNF, IL-7, IL-16, IL-17F, IL-18, IFN- γ , SCF, FGF Basic, and G-CSF (Figure 4F) (Adjusted p < 0.05). Thus, PGN stimulation increased multiple cytokines and chemokines in both 2D and 3D cultures, indicating a robust gram-positive-specific catabolic response, whereas LPS had limited effects.

3.5 | S. aureus Is Detected Intracellularly After 1h of Co-Culture

The growth of *S. aureus* was not affected by the different culture conditions; *C. acnes* however showed a slower growth under low glucose media than Mueller Hinton Broth (Figure S3). Fluorescently labeled *S. aureus* was observed intracellularly within disc cells after a one-hour incubation period at an MOI of 0.01 (Figure S4).

3.6 | Low Bacterial Load Does Not Upregulate Phospho-ERK, JNK, p38 or NFkB

Within treatment groups treated with inhibitors of TLR2 and NOD alone no changes in the expression of pERK, pJNK, pp38 or pNFkB were observed (Figure 5). When cells were treated with either $50\mu g/mL$ PGN, *S. aureus* (MOI 0.01) or *C. acnes* (MOI 0.01) in the absence of inhibitors a small increase in pERK, pJNK, pP38 and pNFkB following PGN treatment was noted, which reached significance for pERK (p=0.0041) and pNFkB (p=0.0011) compared to the non-treated control. Inhibition of TLR2 in combination with PGN treatment still showed a small increase in pERK, pJNK, pP38 and pNFkB, which reached

significance for pERK (p = 0.0008) and pNFkB (p = 0.0006) compared to the inhibited but non-stimulated control. TLR2 inhibition in combination with S. aureus treatment led to a significant decrease (p = 0.0312) in pJNK compared to the non-stimulated control (Figure 5). Inhibition of NOD in combination with PGN treatment showed a small increase in pERK, pJNK, pP38 and pNFkB, which reached significance for pNFkB (p=0.0003) compared to the non-stimulated, inhibited control. Following combined inhibition of TLR and NOD, PGN treatment led to an increase in pERK, pJNK, pP38 and pNFkB which reached significance in pERK (p = 0.0094) and pNFkB (p = 0.0109) compared to the inhibited non-treated control (Figure 5). A significant increase (p = 0.0442) in pJNK was also observed following stimulation with C. acnes compared to the non-stimulated inhibited control (Figure 5). Overall, low bacterial load induced only small increases in MAPK/NF-xB phosphorylation (e.g., pERK, pNFxB), implying that minimal bacterial exposure triggers weak intracellular signaling.

3.7 | Catabolic Factors Were Increased by PGN Stimulation but Down Regulated by Co-Culture With Bacteria

Inhibition of TLR2 or NODin1 as well as the combined inhibition without treatment only resulted in a significant downregulation of CCL5 during NOD inhibition ($p\!=\!0.0071$) compared to the non-inhibited control (Figure 6). Treatment without inhibition with PGN resulted in an increase in TNF, IL-1 α , IL-1Ra, and CCL5 in 2/3 donors (Figure 6). IL-1 β was below the detection limit for the untreated control samples but was induced by PGN stimulation in 2/3 donors. Treatment of cells in monolayer with *S. aureus* (MOI 0.01) in the absence

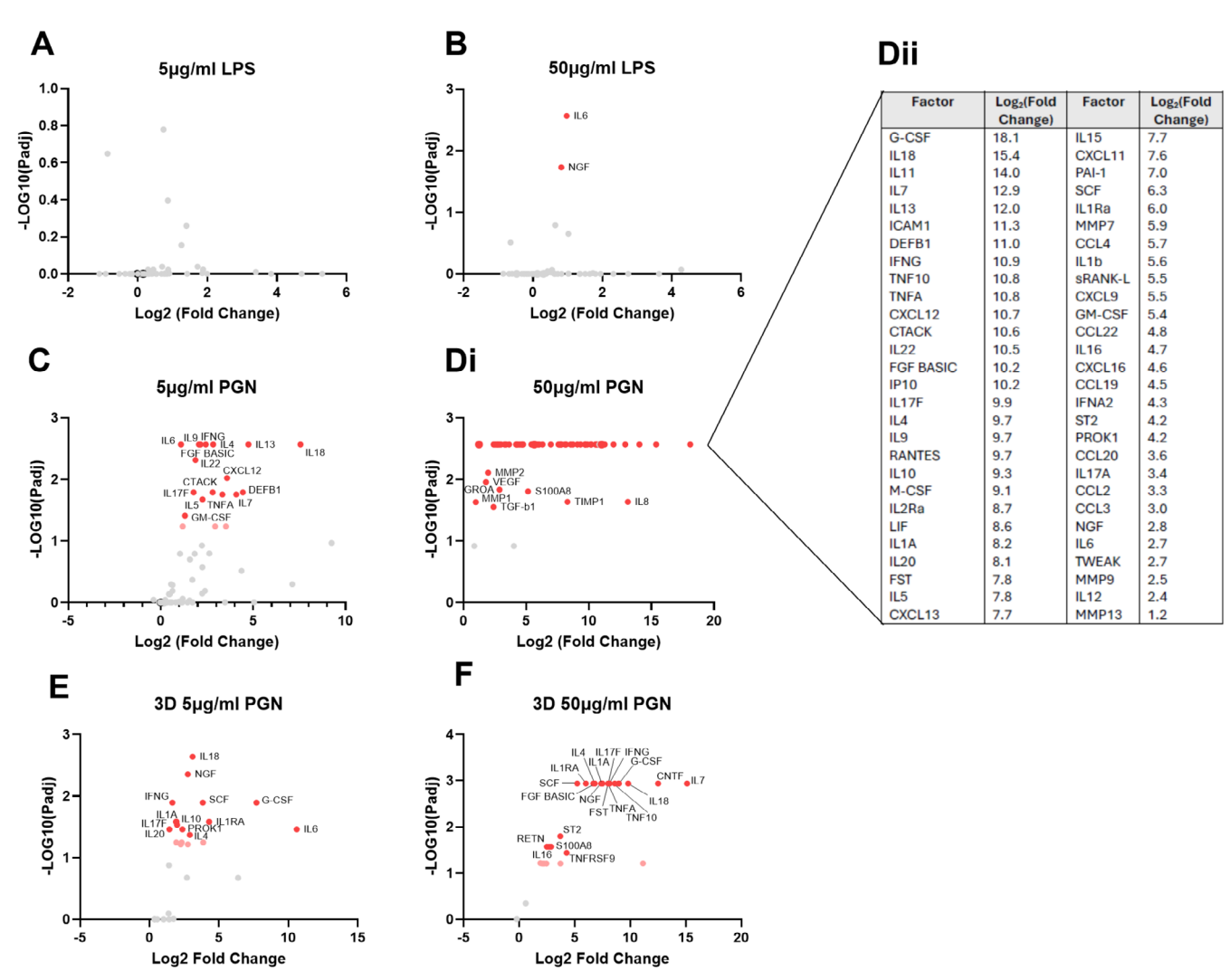


FIGURE 4 | Secretome of human NP cells following exposure to bacterial cell wall components. Volcano plots of secretome determined by multiplex Luminex analysis of human NP cells (N=3 donors, n=3 replicates per donor) stimulated with Lipopolysaccharide (LPS) (A, B) or peptidoglycan (PGN) (C-F). Data was firstly normalized to within donor unstimulated controls and statistical analysis performed with Multiple Mann-Whitney testing, p values corrected for multiple comparisons using the Holm-Sidak Method. Volcano plots represent Log₂(fold change) from unstimulated controls, and $-LOG_{10}$ (Adjusted P). Significant (p < 0.05) increases are indicated by dark red points, and trends (p < 0.1) by pale red points, whilst significant (p < 0.05) decreases are indicated by dark blue points and trends (p < 0.01) by pale blue points. Target labels are included for any significantly affected proteins compared to unstimulated controls. (A) Volcano plot for human NP cells (N=3) in monolayer stimulated with $5 \mu g/mL$ LPS for 48 hin low glucose media under 21% O2 conditions compared to unstimulated controls. (B) Volcano plot for human NP cells (N=3) in monolayer stimulated with $50\mu g/mL$ LPS for $48\,h$ in low glucose media under 21% O₂ conditions compared to unstimulated controls. (C) Volcano plot for human NP cells (N=3) in monolayer stimulated with $5 \mu g/mL$ PGN for 48 h in low glucose media under $21\% O_2$ conditions compared to unstimulated controls. (Di) Volcano plot for human NP cells (N=3) in monolayer stimulated with 50 µg/mL PGN for 48 h in low glucose media under 21% O, conditions compared to unstimulated controls. (Dii) Table of targets with -Log₁₀(Adj P)=2.56 (AdjP=0.0027) together with their respective with Log₃(Fold Change). (E) Volcano plot for human NP cells (N=3) resuspended in alginate and re differentiated for 2 weeks in low glucose serum free media under physioxia (5% O₂), prior to stimulation with 5 μg/mL PGN for 72h compared to unstimulated controls. (F) Volcano plot for human NP cells (N=3) resuspended in alginate and re differentiated for 2 weeks in low glucose serum free media under physioxia (5% O₂), prior to stimulation with 50 µg/ mL PGN for 72 h compared to unstimulated controls.

of inhibitors resulted in a significant decrease of IL-1Ra (p=0.0307), CCL5 (p=0.0160) and VEGF (p=0.0011), compared to the control (Figures 6 and S5). Exposure of NP cells to *C. acnes* (MOI 0.01) in the absence of inhibitors showed a significant decrease in VEGF (p=0.0068) and CXCL10 (p=0.0144) compared to the non-inhibited untreated control. Inhibition of TLR2 in combination with PGN did not inhibit the actions of PGN, with increases in TNF, IL-1 α , IL-1Ra and CCL5 in 2/3 donors observed (Figure 6). Treatment with *S*.

aureus in combination with TLR2 inhibition showed a significant decrease in IL-1 α (p=0.0282), CCL5 (p=0.0352) and VEGF (p=0.0059) compared to the non-treated TLR2 inhibited control (Figure 6). *C. acnes* treatment combined with TLR2 inhibition showed a significant decrease in IL-1 α (p=0.0301), CCL5 (p=0.0428), VEGF (p=0.0007) and ICAM (p=0.0435) compared to the control (Figures 6 and S5). Inhibition of NOD in combination with PGN treatment resulted in an increase in CCL5 in 2 donors and a significant increase in TNF

JOR Spine, 2025 9 of 15

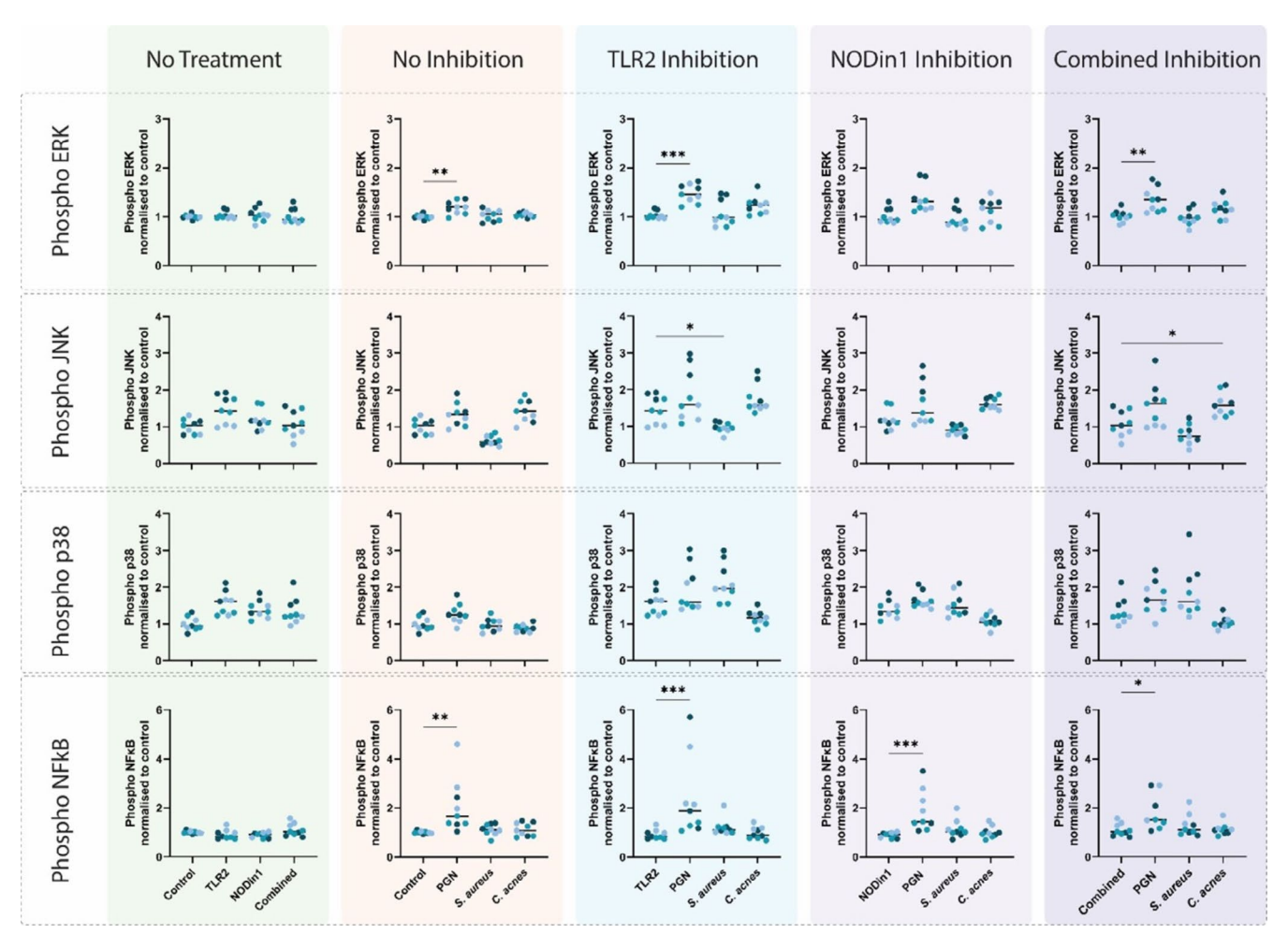


FIGURE 5 | Stimulation of NP cells with *S. aureus* and *C. acnes* combined with inhibitors. In cell-ELISA was used to measure phospho-ERK, JNK, p38 and NFkB. Cells in monolayer under hypoxia were left to attach overnight before treatment with the inhibitors for TLR2, NODin1 and both combined for 24 h. Followed by the inhibition was treatment with $50\mu g/mL$ PGN, *S. aureus* (MOI 0.01) and *C. acnes* (MOI 0.01) for 2 h in combination with the inhibitors. The different shades of blue represent the different donors (N=3 donors, n=3 wells, (stats performed on n=9)). All the measured concentrations were normalized to the non-treated control. The No treatment graphs, show the different levels of phospho ERK, JNK, p38 and NFkB for cells only inhibited but not treated with a stimulant. No Inhibition shows treatment with PGN, *S. aureus* and *C. acnes* without inhibitors and TLR2, NODin1 and Combined Inhibition show the treatment combined with the inhibition. Statistical analysis was performed using Kruskal Wallis multiple comparison against the control group of each treatment (p=0.05).

(p = 0.0246) and IL-1Ra (p = 0.0301) compared to the NODin1inhibited untreated control. A significant decrease of VEGF was detected in NOD inhibited samples treated with *S. aureus* (p = 0.0123) and C. acnes (p = 0.0421) compared to the control (Figure 6). Furthermore, the inhibition of NOD in combination with C. acnes exposure led to a significant decrease in CXCL10 (p = 0.0361) (Figure S5). Combination of TLR2 and NOD inhibition in combination with PGN treatment resulted in a non-significant increase in IL-1Ra, CCL5 and VEGF, and a significant increase in TNF (p=0.0027) compared to the inhibited untreated control (Figure 6). The combined inhibition together with S. aureus treatment resulted in significant decreases in CCL5 (p = 0.0209), VEGF (p = 0.0427), IL-7 (p = 0.0074) and CXCL10 (p = 0.0279) compared to the control. C. acnes treatment combined with inhibition of TLR2, and NODs resulted in a significant decrease in IL-1 α (p = 0.0033), VEGF (p = 0.0078), and CXCL10 (p = 0.0315) compared to the control (Figure 6). No changes in any treatment conditions or inhibitors were detected in IL-4, IL-18 and CCL4 (Figure S5).

MMP9 concentrations were below detection limits, whilst MMP3 was above the limit of detection and thus could not be quantified. To conclude, PGN increased TNF, IL-1 α and IL-1Ra, whereas low-MOI *C. acnes* and *S. aureus* suppressed VEGF, CXCL10 and CCL5; these effects were variably altered by TLR2/NOD2 inhibition, suggesting receptor-specific but incomplete pathway dependence.

4 | Discussion

This study investigated bacterial components' presence within non-herniated human IVDs, aiming to distinguish between perioperative contamination and true in vivo colonization. Immunohistochemical staining detected *C. acnes* and *S. aureus* within IVD tissue, locating both bacterial antigen staining within cellular boundaries in human NP cells. Correlations between *C. acnes* and specific catabolic markers, notably NOD2, MMP3, and GSDMD, were also observed. A

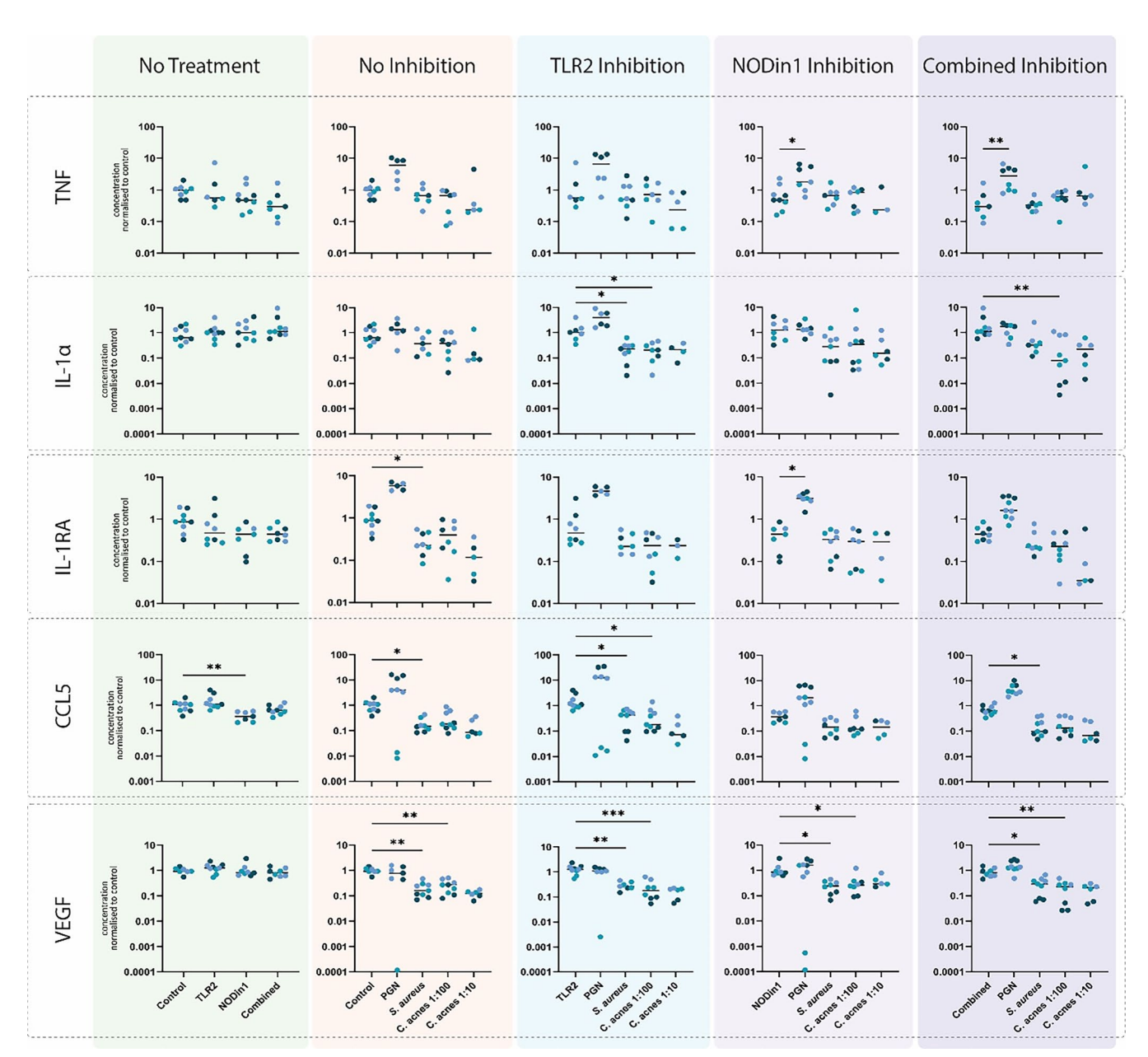


FIGURE 6 | Cytokine expression following treatment with PGN, *S. aureus* and *C. acnes* in the presence of inhibitors. Cells in monolayer were left to attach overnight in a low oxygen chamber before stimulating them with TLR2 inhibitor, NODin1 inhibitor and a combination of the inhibitors for 24 h. Following the stimulation period cells were exposed to $50 \mu g/mL$ PGN, *S. aureus* (MOI 0.01) or *C. acnes* (MOI 0.01, MOI 0.1) for 2 h followed by a PBS wash and the addition of fresh media supplemented with the inhibitors. The secretome was collected and a Luminex assay was performed. Concentrations of each cytokine are shown normalized to the non-stimulated non-treated control. Statistical analysis was not performed for *C. acnes* at an MOI 0.1 as the experiment was only performed in biological duplicates. Kruskal-Wallis multiple comparison test was used to compare the treatments with the stimulation control (p = 0.05). Different shades represent different donors (N = 3 donors, N = 3 wells, (stats performed on N = 9)).

low p value ($p\!=\!0.069$) for C. acnes and IL-1 β suggested a potential correlation, though increased sample numbers might confirm this finding. Experiments under disc-like conditions demonstrated bacterial survival, particularly for C. acnes, while exposure to bacterial cell wall components induced a catabolic response in NP cells, although a low bacterial load mimicking physiological levels did not alter catabolic cytokine expression.

The concept of a disc microbiome has spurred debate, challenging the historical view of the IVD as a sterile environment [23–25]. *C. acnes* has drawn particular interest, partly due to its

role as a commensal and as an opportunistic pathogen in the skin, soft tissues, and medical device-related infections [26, 27]. Traditional bacterial detection techniques like microbial culture and NGS cannot rule out contamination, while immunohistochemistry offers a more precise localization of bacteria within cellular boundaries. This study excluded herniated discs which were extruded or sequestered, using only discs with an intact annulus, focusing on degenerated yet contained discs to minimize contamination risks and assess in vivo bacterial presence. Detecting *C. acnes* and *S. aureus* antigens within cellular boundaries in NP and AF cells offers compelling evidence for an intrinsic disc microbiome, with implications for disc health and

JOR Spine, 2025 11 of 15

pathology. While IHC showed bacterial antigen signals within cellular boundaries, this cannot definitively confirm intracellular localization or active colonization. Surface-adherent or phagocytosed antigen remnants remain possible explanations. Future studies using 16S rRNA in situ hybridization combined with confocal Z stacks on thick tissue sections could help unravel this remaining question, and support true intracellular localization.

Bacteria may enter the IVD through various routes, including the CEP or the AF, where microtears or disruptions could serve as entry points. Furthermore, bacterial colonization may occur prenatally, with bacteria potentially present in the disc from early developmental stages, or through hematogenous spread after birth. Immunostaining in our study revealed the localization of *C. acnes* and *S. aureus* antigens within disc cell boundaries, suggesting bacterial internalization via phagocytosis or the presence of intracellular remnants. This warrants further investigation into the mechanisms of bacterial persistence and localization within the IVD.

Importantly, our findings show bacterial components across a range of age groups, degeneration grades, and Modic changes without significant differences suggesting that these bacteria might not solely play a pathogenic role but could also have a commensal or homeostatic function within the disc environment. This interpretation highlights the need to consider that certain bacteria may participate in maintaining disc health rather than solely promoting degeneration.

Bacterial components such as LPS and PGN are known to trigger a robust catabolic response in human NP cells, inducing the expression of the catabolic cytokine IL-1 β , matrix-degrading enzymes MMP13 and ADAMTS4, and neurotrophic factors like NGF and BDNF through the activation of the TLR2 heterodimer and the TLR4 homodimer [13, 28, 29]. The $50\,\mu\text{g/mL}$ PGN treatment represents a supraphysiologic stimulus and was used as a positive control to elicit a broad catabolic response, whereas lower doses (e.g., $5\,\mu\text{g/mL}$) are likely more reflective of physiologic bacterial exposure within the IVD. However, as the extent of bacterial colonization within the disc is unknown, all doses should be regarded as estimates. Consistent with previous studies, our in vitro experiments showed a significant catabolic response, especially with PGN treatment, highlighting the potential effects of bacterial presence in the disc environment.

Immunohistochemical staining revealed a positive correlation between *C. acnes* and MMP3, as well as between *C. acnes* and GSDMD, a protein involved in pyroptosis [30]. However, no correlation was found between bacterial components' presence and the positivity rate of TLRs, suggesting the involvement of other mechanisms in driving this catabolic response beyond TLR activation alone. Indeed, TLRs may not be the dominant driver in the catabolic response to bacteria, as bacterial antigens were detected within cellular boundaries. Mengis et al. reported elevated TLR2 expression in cells from patients with Modic change type 1 and in catabolic conditions, highlighting their pro-inflammatory and pro-catabolic roles, which may contribute to disc degeneration and MCs [10]. Similarly, Schmid et al. demonstrated in a study the involvement of the TLR2/4 pathways in inducing a catabolic response upon stimulation with *C*.

acnes, but only in a subgroup of patients further supporting the involvement of other pathways [12].

NOD2 is an intracellular pattern recognition receptor sensing muramyl dipeptide, a component of bacterial PGN. It plays a role in inflammatory responses, particularly in epithelial cells and immune cells, where it activates NFkB and MAPK pathways leading to cytokine production [31, 32]. While NOD2 has not been previously reported in human NP cells, our immunohistochemical analysis detected NOD2 and showed its presence in the disc, with a positive correlation between NOD2 and *C. acnes* positivity. This finding points to a potentially important role for NOD2 in the disc's response to bacterial components' presence, further supporting the notion that multiple receptors contribute to bacterial detection and the ensuing catabolic activity in the disc. It furthermore suggests that NP cells play an active role in immune surveillance within the disc environment and act as immune-like responders.

Despite these findings, the inhibition of TLR2 and NODs in the presence of PGN did not affect the phosphorylation of ERK, JNK, p38, or NFkB, nor did the inhibition alter the expression of cytokines such as TNF and IL- 1α . This lack of inhibition suggests that either other signaling pathways may be compensating for the absence of TLR and NOD activation, or the inhibitors failed to inhibit the receptors fully. However, the concentration utilized for NODin1 inhibition was shown to be effective in reducing IL-1 β secretion in mice CD8 T cells upon infection [33]. TLR2 inhibition has also been shown to decrease the release of pro-inflammatory factors in BV2 microglial cells in a concentration that was applied in our study [34]. This points to the involvement of additional pathways, such as NLRP3 inflammasomes, which are activated by microbial stimuli and have been implicated in NP cell pyroptosis [30]. This aligns with our finding of a correlation between the positivity rate for GSDMD and C. acnes using immunohistochemistry. GSDMD is a key effector of pyroptosis, supporting the hypothesis that NLRP3mediated inflammasome activation could contribute to the observed catabolic response.

Another potential pathway might involve C-type lectin receptors (CLRs), a family of pattern recognition receptors (PRRs) that detect specific carbohydrate structures commonly found on pathogens, including bacteria. CLRs recognize glycans such as mannose, fucose, and N-acetylglucosamine, which are components of bacterial peptidoglycan [35–38]. Notable CLRs include DC-SIGN, Dectin-1, and the mannose receptor, primarily expressed on antigen-presenting cells like macrophages and dendritic cells. Upon activation, CLRs initiate signaling cascades that lead to cytokine production and immune cell recruitment to fight infections [39]. However, it remains unknown whether CLRs are expressed within the IVD, representing an avenue for further investigation.

Co-culture of NP cells with a low bacterial load (MOI 0.01, representing 1 bacteria to 100 NP cells at the time of addition) which was predicted to mimic physiological levels following replication at the rates observed within these culture conditions, showed no significant activation of these pathways, aligning with the notion that a higher bacterial load may be required to induce a stronger response. Interestingly, we observed a strong

downregulation of IL-1Ra, CCL5 and VEGF protein expression in cells stimulated with a low load of *S. aureus*. Furthermore, VEGF was strongly downregulated upon stimulation with a low load of *C. acnes*. The degenerated NP cells used for this experiment already have a higher catabolic cytokine expression than healthy cells [40] and, would be expected to express VEGF at a higher level. Even when treated with PGN, one donor showed a decrease in CCL5 and IL-1Ra compared to the non-treated control, indicating donor variability. Notably, the other two donors did not show an increase in VEGF, implying that the VEGF upregulation may occur later as a downstream effect of the rise in catabolic cytokines [41].

The observed cytokine expression levels might also be a consequence of the study design. First, we did not capture cytokine release during the initial 2-h infection period, which may have resulted in missing early catabolic responses triggered by bacterial internalization. Furthermore, the internalization rate of bacteria by NP cells remains unknown, leading to uncertainty in determining the precise MOI specific to intracellular bacteria. Previous studies with higher MOI (100) reported robust activation of ERK, JNK, p38, and NFkB in human NP cells derived from patients with degenerate discs after C. acnes infection for different culturing periods peaking at 4 h [42]. Elevated IL-6 and IL-8 levels in NP cells of IVDs from degenerate patient samples have also been associated with higher bacterial loads (MOI 100) after 24h in vitro stimulation [13], suggesting that bacterial load and duration of exposure may play critical roles in modulating NP cell responses. It is important to note that bacteria multiply more rapidly than human cells, meaning the MOI will shift over time as bacterial populations grow. Additionally, culture conditions play a significant role in experimental outcomes. While previous studies utilized HG F12 DMEM media supplemented with 10%-15% FCS at 37°C, 5% CO_2 and 21% O_2 , the current study was conducted in a low-oxygen (5%) glovebox with LG DMEM serum free media supplemented with 1% ITS-X, which more closely replicates the disc environment.

Another important factor to consider is the bacterial strains used in experimental designs or detected in studies. Over the past decade, biochemical, transcriptomic, and proteomic analyses have shown that different phylotypes of C. acnes vary in their inflammatory potential and expression of putative virulence factors [43]. For instance, C. acnes is the most prevalent bacterium in the human skin microbiome, with no significant difference in load between healthy skin and acne-affected skin. However, inflammatory acne is believed to be triggered by an imbalance in the skin microbiota, specifically due to the selection of certain C. acnes phylotypes [44]. Additionally, different C. acnes types have been identified at different body sites. While phylotype IA was mostly identified in severe acne, phylotypes IB and II, types IB and IC have been associated with colonization of the prostate, urinary tract, and orthopedic equipment [9, 44, 45]. A study examining the phylotypes of C. acnes detected in IVDs reported that 18 out of 60 analyzed samples were positive for C. acnes microbial cultures. Among these 18 strains, 39% belonged to phylotype II, 33% to type IA1, 6% to type IB1, and 22% to phylotype III. The study further observed that rabbits injected with C. acnes type IB or II strains exhibited significantly decreased T1-weighted imaging (T1WI) and increased T2-weighted imaging (T2WI) signals at 8 weeks, whereas those injected with

strain III showed hypointense signals on both T1WI and T2WI, highlighting differences between the phylotypes [46]. Schmid et al. used a clinical $\it C.$ acnes isolate from spinal infection and ATCC purchased strain isolated from facial acne to treat human NP cells in vitro [12]. They reported higher gene expression levels of IL-1 $\it \beta$, IL-6 and IL-8 for the ATCC strains as well as higher protein levels in the secretome for IL-6 and IL-8 (IL-1 $\it \beta$ was not reported) [12]. Cytokine expression however was not significantly upregulated upon treatment with either $\it C.$ acnes strain due to high fluctuations between their 4 donors [12]. Indicating again donor variability and the possibility of responders and non-responders.

Similarly, to *C. acnes*, *S. aureus* is a normal component of the skin microbiome, can cause a wide range of diseases depending on the virulence factors it carries, from mild skin infections to life-threatening conditions such as pneumonia and sepsis [47]. In this study, laboratory strains of bacteria were used: *C. acnes* isolated from acne-affected skin and *S. aureus* from the conjunctiva. It is important to note that the virulence factors of these laboratory strains may differ from strains isolated directly from infection sites.

5 | Study Limitations

A key limitation is that IHC cannot distinguish true intracellular bacteria from phagocytosed antigen, and 16S rRNA in situ hybridisation could be used in combination with thicker sections and confocal microscopy to confirm localisation of bacterial RNA, indicating recent bacterial presence. Another limitation of this study is the focus on S. aureus and C. acnes, potentially overlooking the influence of other microbial species suggested by recent 16S-Sequencing studies to be present in the IVD. Furthermore, the study is limited by the inability to distinguish bacterial strains using IHC. Future studies should aim to employ more specific methods, such as in situ hybridisation or sequencing-based techniques, to determine whether distinct bacterial strains/phylotypes are present. Additionally, cytokine expression patterns observed may be influenced by the study design. Specifically, cytokine release was not captured during the initial 2-h infection period, possibly missing early catabolic responses triggered by bacterial internalization. The bacterial internalization rate by NP cells is also undetermined, creating uncertainty in defining the precise MOI for intracellular bacteria. Moreover, while in vitro monolayer cultures allowed for controlled experimentation, they lack the complex 3D architecture and unique microenvironment of the human IVD, potentially limiting the direct applicability of these findings to in vivo conditions. Finally, as analyses were based on three donors, the findings should be considered exploratory and require confirmation in larger cohorts.

6 | Conclusion

This study provides compelling evidence of bacterial components' presence within non-herniated human IVDs, specifically *C. acnes* and *S. aureus*. Immunohistochemical detection not only localizes bacteria within NP cells but also reveals significant correlations between *C. acnes* and catabolic markers such

JOR Spine, 2025 13 of 15

as MMP3, GSDMD, and NOD2. This suggests that NP cells may actively participate in immune surveillance. The involvement of NOD2 points to previously unrecognized intracellular pathways contributing to bacterial detection and subsequent inflammatory responses. Our findings suggest that TLRs may not be the dominant receptors in this process, indicating the role of other mechanisms, such as the NLRP3 inflammasome or potentially CLRs, which could drive the catabolic response, although this requires further investigation. While low bacterial loads did not trigger significant activation of the MAPK or NF-kB pathways, previous studies with higher bacterial loads highlight the importance of infection intensity and duration in modulating NP cell responses. These results underscore the complex interplay of multiple receptors and pathways in the disc's immune response to bacteria and pave the way for further exploration of targeted therapeutic interventions for disc-related pathologies.

Author Contributions

C.L.L.M., B.G., L.G.A., M.L. contributed to the conception and design of the study and funding acquisition; A.N., E.K. contributed to the acquisition of laboratory data; A.N., and C.L.L.M. performed data analysis; A.N., E.K., L.G.A., M.L., B.G., C.L.L.M. contributed to the interpretation of the data; A.N. drafted the manuscript, All authors critically revised the manuscript. C.L.L.M. coordinated the study. All authors read and approved the final manuscript.

Acknowledgments

We thank the Marie Skłodowska Curie International Training Network (ITN) "Disc4All" for financial support. Our sincere thanks go to the surgeons at Northern General Hospital and Claremont Hospital for their invaluable efforts in collecting tissue samples, as well as to the patients for their donations. We also extend our gratitude to Shreya Srinivas and Jo McKay for their assistance in the classification of samples according to Modic changes.

Disclosure

The funder had no role in the manuscript.

Conflicts of Interest

Prof. Alexopoulos and E. Kanelis work at Protavio.

Data Availability Statement

The data that support the findings of this study are available from the corresponding author upon reasonable request.

References

- 1. M. Mirzaeipoueinak, H. S. Mordechai, S. S. Bangar, M. Sharabi, J. L. Tipper, and J. Tavakoli, "Structure-Function Characterization of the Transition Zone in the Intervertebral Disc," *Acta Biomaterialia* 160 (2023): 164–175.
- 2. M. L. Ferreira, K. de Luca, L. M. Haile, et al., "Global, Regional, and National Burden of Low Back Pain, 1990-2020, Its Attributable Risk Factors, and Projections to 2050: A Systematic Analysis of the Global Burden of Disease Study 2021," *Lancet Rheumatology* 5 (2023): e316–e329.
- 3. A. Stirling, T. Worthington, M. Rafiq, P. A. Lambert, and T. S. J. Elliott, "Association Between Sciatica and *Propionibacterium acnes*," *Lancet* 357 (2001): 2024–2025.

- 4. S. Rajasekaran, D. C. R. Soundararajan, C. Tangavel, et al., "Human Intervertebral Discs Harbour a Unique Microbiome and Dysbiosis Determines Health and Disease," *European Spine Journal* 29 (2020): 1621–1640.
- 5. T. Mengis, N. Zajac, L. Bernhard, et al., "Intervertebral Disc Microbiome in Modic Changes: Lack of Result Replication Underscores the Need for a Consensus in Low-Biomass Microbiome Analysis," *JOR Spine* 7 (2024): e1330.
- 6. T. Mengis, N. Zajac, L. Bernhard, et al., "Intervertebral Disc Microbiome in Modic Changes: Lack of Result Replication Underscores the Need for a Consensus in Low-Biomass Microbiome Analysis," *JOR Spine* 7 (2024): e1330.
- 7. S. Rajasekaran, D. C. R. Soundararajan, C. Tangavel, et al., "Human Intervertebral Discs Harbour a Unique Microbiome and Dysbiosis Determines Health and Disease," *European Spine Journal* 29 (2020): 1621–1640.
- 8. V. Agarwal, S. R. Golish, and T. F. Alamin, "Bacteriologic Culture of Excised Intervertebral Disc From Immunocompetent Patients Undergoing Single Level Primary Lumbar Microdiscectomy," *Journal of Spinal Disorders & Techniques* 24 (2011): 397–400.
- 9. M. N. Capoor, F. Ruzicka, J. E. Schmitz, et al., "*Propionibacterium acnes* Biofilm Is Present in Intervertebral Discs of Patients Undergoing Microdiscectomy," *PLoS One* 12 (2017): e0174518.
- 10. T. Mengis, L. Bernhard, A. Nüesch, et al., "The Expression of Toll-Like Receptors in Cartilage Endplate Cells: A Role of Toll-Like Receptor 2 in Pro-Inflammatory and pro-Catabolic Gene Expression," *Cells* 13 (2024): 1402.
- 11. M. Klawitter, M. Hakozaki, H. Kobayashi, et al., "Expression and Regulation of Toll-Like Receptors (TLRs) in Human Intervertebral Disc Cells," *European Spine Journal* 23 (2014): 1878–1891.
- 12. B. Schmid, O. Hausmann, W. Hitzl, Y. Achermann, and K. Wuertz-Kozak, "The Role of Cutibacterium Acnes in Intervertebral Disc Inflammation," *Biomedicine* 8 (2020): 186.
- 13. D. G. Bisson, M. Mannarino, R. Racine, and L. Haglund, "For Whom the Disc Tolls: Intervertebral Disc Degeneration, Back Pain and Toll-Like Receptors," *European Cells and Materials* 41 (2021): 355–369.
- 14. G. Tang, X. Han, Z. Lin, et al., "Propionibacterium acnes Accelerates Intervertebral Disc Degeneration by Inducing Pyroptosis of Nucleus Pulposus Cells via the ROS-NLRP3 Pathway," Oxidative Medicine and Cellular Longevity 2021 (2021): 4657014.
- 15. W. Strober and T. Watanabe, "NOD2, an Intracellular Innate Immune Sensor Involved in Host Defense and Crohn's Disease," *Mucosal Immunology* 4 (2011): 484–495.
- 16. C. L. Le Maitre, C. L. Dahia, M. Giers, et al., "Development of a Standardized Histopathology Scoring System for Human Intervertebral Disc Degeneration: An Orthopaedic Research Society Spine Section Initiative," *JOR Spine* 4 (2021): e1167.
- 17. A. Binch, J. Snuggs, and C. L. Le Maitre, "Immunohistochemical Analysis of Protein Expression in Formalin Fixed Paraffin Embedded Human Intervertebral Disc Tissues," *JOR Spine* 3 (2020): e1098.
- 18. A. Nüesch, M. P. Ferri, and C. L. Le Maitre, "Application and Validation of Semiautomatic Quantification of Immunohistochemically Stained Sections for Low Cellular Tissue Such as Intervertebral Disc Using QuPath," *JOR Spine* 8 (2025): e70054.
- 19. S. Basatvat, F. C. Bach, M. N. Barcellona, et al., "Harmonization and Standardization of Nucleus Pulposus Cell Extraction and Culture Methods," *JOR Spine* 6 (2023): e1238.
- 20. S. Basatvat, F. C. Bach, M. N. Barcellona, et al., "Harmonization and Standardization of Nucleus Pulposus Cell Extraction and Culture Methods," *JOR Spine* 6 (2023): e1238.

- 21. H. Li, J. Wang, F. Li, G. Chen, and Q. Chen, "The Influence of Hyperosmolarity in the Intervertebral Disc on the Proliferation and Chondrogenic Differentiation of Nucleus Pulposus-Derived Mesenchymal Stem Cells," *Cells, Tissues, Organs* 205 (2018): 178–188.
- 22. C. Poussin, C. Mathis, L. G. Alexopoulos, et al., "The Species Translation Challenge—A Systems Biology Perspective on Human and Rat Bronchial Epithelial Cells," *Scientific Data* 1, no. 1 (2014): 1–14.
- 23. S. Dudli, S. Miller, S. Demir-Deviren, and J. C. Lotz, "Inflammatory Response of Disc Cells Against *Propionibacterium acnes* Depends on the Presence of Lumbar Modic Changes," *European Spine Journal* 27 (2018): 1013–1020.
- 24. I. Heggli, T. Mengis, C. J. Laux, et al., "Low Back Pain Patients With Modic Type 1 Changes Exhibit Distinct Bacterial and Non-Bacterial Subtypes," *Osteoarthritis and Cartilage Open* 6 (2024): 100434.
- 25. C. Manniche and S. O'Neill, "New Insights Link Low-Virulent Disc Infections to the Etiology of Severe Disc Degeneration and Modic Changes," *Future Science OA* 5 (2019): FSO389.
- 26. S. Ahmed-Yahia, J. W. Decousser, C. H. Flouzat-Lachaniette, et al., "Is the Discopathy Associated With Modic Changes an Infectious Process? Results From a Prospective Monocenter Study," *PLoS One* 14 (2019): e0221030.
- 27. P. Fritzell, C. Welinder-Olsson, B. Jönsson, et al., "Bacteria: Back Pain, Leg Pain and Modic Sign—A Surgical Multicentre Comparative Study," *European Spine Journal* 28 (2019): 2981–2989.
- 28. M. B. Ellman, J. S. Kim, H. S. An, et al., "Toll-Like Receptor Adaptor Signaling Molecule MyD88 on Intervertebral Disk Homeostasis: In Vitro, Ex Vivo Studies," *Gene* 505 (2012): 283–290.
- 29. E. Krock, D. H. Rosenzweig, J. B. Currie, D. G. Bisson, J. A. Ouellet, and L. Haglund, "Toll-Like Receptor Activation Induces Degeneration of Human Intervertebral Discs," *Scientific Reports* 7 (2017): 17184.
- 30. G. Tang, X. Han, Z. Lin, et al., "Propionibacterium acnes Accelerates Intervertebral Disc Degeneration by Inducing Pyroptosis of Nucleus Pulposus Cells via the ROS-NLRP3 Pathway," Oxidative Medicine and Cellular Longevity 2021 (2021): 4657014.
- 31. R. Caruso, N. Warner, N. Inohara, and G. Núñez, "NOD1 and NOD2: Signaling, Host Defense, and Inflammatory Disease," *Immunity* 41 (2014): 898–908.
- 32. M. Proell, S. J. Riedl, J. H. Fritz, A. M. Rojas, and R. Schwarzenbacher, "The nod-Like Receptor (NLR) Family: A Tale of Similarities and Differences," *PLoS One* 3 (2008): e2119.
- 33. P. Thakker, A. Ariana, S. Hajjar, D. Cai, D. Rijal, and S. Sad, "XIAP Promotes the Expansion and Limits the Contraction of CD8 T Cell Response Through Cell Extrinsic and Intrinsic Mechanisms Respectively," *PLoS Pathogens* 19 (2023): e1011455.
- 34. X. Yan, Q. Li, S. Wu, et al., "Acrylamide Induces the Activation of BV2 Microglial Cells Through TLR2/4-Mediated LRRK2-NFATc2 Signaling Cascade," *Food and Chemical Toxicology* 176 (2023): 113775.
- 35. M. E. Mnich, R. van Dalen, and N. M. van Sorge, "C-Type Lectin Receptors in Host Defense Against Bacterial Pathogens," *Frontiers in Cellular and Infection Microbiology* 10 (2020): 309.
- 36. M. van der Vlist, L. de Witte, R. D. de Vries, et al., "Human Langerhans Cells Capture Measles Virus Through Langerin and Present Viral Antigens to CD4 ⁺ T Cells but Are Incapable of Cross-Presentation," *European Journal of Immunology* 41 (2011): 2619–2631.
- 37. G. Raes, L. Brys, B. K. Dahal, et al., "Macrophage Galactose-Type C-Type Lectins as Novel Markers for Alternatively Activated Macrophages Elicited by Parasitic Infections and Allergic Airway Inflammation," *Journal of Leukocyte Biology* 77 (2005): 321–327.
- 38. T. B. H. Geijtenbeek, R. Torensma, S. J. van Vliet, et al., "Identification of DC-SIGN, a Novel Dendritic Cell–Specific ICAM-3 Receptor That Supports Primary Immune Responses," *Cell* 100 (2000): 575–585.

- 39. B. K. Patterson, A. Landay, J. N. Siegel, et al., "Susceptibility to Human Immunodeficiency Virus-1 Infection of Human Foreskin and Cervical Tissue Grown in Explant Culture," *American Journal of Pathology* 161 (2002): 867–873.
- 40. S. Han, Y. Zhang, X. Zhang, et al., "Single-Cell RNA Sequencing of the Nucleus Pulposus Reveals Chondrocyte Differentiation and Regulation in Intervertebral Disc Degeneration," *Frontiers in Cell and Development Biology* 10 (2022): 824771.
- 41. M. V. Risbud and I. M. Shapiro, "Role of Cytokines in Intervertebral Disc Degeneration: Pain and Disc Content," *Nature Reviews Rheumatology* 10 (2014): 44–56.
- 42. Y. Lin, Y. Jiao, Y. Yuan, et al., "Propionibacterium Acnes Induces Intervertebral Disc Degeneration by Promoting Nucleus Pulposus Cell Apoptosis via the TLR2/JNK/Mitochondrial-Mediated Pathway Article," Emerging Microbes & Infections 7 (2018): 1–8.
- 43. C. Mayslich, P. A. Grange, N. Dupin, and H. Brüggemann, "Cutibacterium Acnes as an Opportunistic Pathogen: An Update of Its Virulence-Associated Factors," *Microorganisms* 9 (2021): 1–21.
- 44. C. Paugam, S. Corvec, M. Saint-Jean, et al., "Propionibacterium acnes Phylotypes and Acne Severity: An Observational Prospective Study," Journal of the European Academy of Dermatology and Venereology 31 (2017): e398–e399.
- 45. S. Tomida, L. Nguyen, B. H. Chiu, et al., "Pan-Genome and Comparative Genome Analyses of *Propionibacterium acnes* Reveal Its Genomic Diversity in the Healthy and Diseased Human Skin Microbiome," *MBio* 4 (2013): e00003–e00013.
- 46. W. Lan, X. Wang, X. Tu, X. Hu, and H. Lu, "Different Phylotypes of Cutibacterium Acnes Cause Different Modic Changes in Intervertebral Disc Degeneration," *PLoS One* 17 (2022): e0270982.
- 47. G. Y. C. Cheung, J. S. Bae, and M. Otto, "Pathogenicity and Virulence of *Staphylococcus aureus*," *Virulence* 12 (2021): 547–569.

Supporting Information

Additional supporting information can be found online in the Supporting Information section. **Figure S1:** Project overview. **Table S1:** Donors used for Immunohistochemical Staining. **Table S2:** Target antibodies used for immunohistochemical staining. **Table S3:** Donors for in vitro Experiments. **Table S4:** List of analyzed proteins. **Figure S2:** Immunohistochemical staining for catabolic factors. **Figure S3:** Growth curve of bacteria in different growth-media. **Figure S4:** Confocal image of intracellular *S. aureus*. **Figure S5:** Cytokine expression following treatment with PGN, *S. aureus* and *C. acnes* in combination with inhibitors.

JOR Spine, 2025 15 of 15